Available online at www.sciencedirect.com
ScienceDirect
Advances in Water Resources 31 (2008) 661–673
Advances in Water Resources
www.elsevier.com/locate/advwatres

Nonequilibrium effects in models of three-phase flow in porous media

Ruben Juanes *

Department of Civil and Environmental Engineering, Massachusetts Institute of Technology, 77 Massachusetts Avenue, Room 48-319, Cambridge, MA 02139, USA

Received 28 January 2007; received in revised form 19 December 2007; accepted 21 December 2007
Available online 26 January 2008

Abstract

In this paper we extend to three-phase flow the nonequilibrium formalism proposed by Barenblatt and co-workers for two-phase porous media flow. The underlying idea is to include nonequilibrium effects by introducing a pair of effective water and gas saturations, which are linked to the actual saturations by a local evolution equation. We illustrate and analyze how nonequilibrium effects lead to qualitative and quantitative differences in the solution of the three-phase flow equations.

Keywords: Porous media; Multiphase flow; Dynamic relative permeability; Dynamic capillary pressure; Nonequilibrium models; Elliptic regions

1. Introduction

The importance of multiphase flow in porous media has long been recognized in many fields [1–5]. More specifically, a good description of three-phase flow is essential in practical applications like enhanced oil recovery, environmental remediation of the unsaturated zone, and geological CO_2 storage in depleted oil and gas reservoirs.

Traditional formulations of multiphase flow describe macroscopic fluid fluxes with a straightforward extension—first proposed by Muskat [6]—of Darcy's equation for single-phase flow. It is well known that, unlike in the single-phase case [7], this extension cannot be rigorously obtained from first principles [8]. The multiphase extension of Darcy's equation may be described as a quasi-linear relation, because the fluid flux depends linearly on the "driving force", which includes viscous, capillary, and gravity forces, and all the nonlinearity is agglutinated in the relative permeability and capillary pressure functions.

It has long been recognized that relative permeability and capillary pressure functions are not unique functions of saturation. They must be treated as functionals that depend, at the very least, on saturation history and saturation path [9–13]. This type of dependence is clearly supported by pore-scale simulations [14–21] and laboratory experiments [22–24]. Moreover, a Darcy-type formulation neglects the viscous coupling among flowing phases [25–28] and does not account for the dependence on flow regime [29–32], which sets the time scales of displacement processes at the pore level [33–36].

In an attempt to remedy this situation, alternatives to Darcy-type formulations have been proposed. Here, we concentrate on continuum models that include so-called "dynamic" or "nonequilibrium" effects. Based on volume averaging of the microscopic equations of conservation of mass and momentum, Hassanizadeh and Gray identified that additional terms should be present in the macroscopic equations [8,37,38]. In particular, they introduced the concept of dynamic capillary pressure, which has been the subject of intense experimental [39–42], modeling [42–49] and theoretical research [50–58].

A different but related model was proposed by Barenblatt and co-workers using more heuristic arguments [59–62] (see also [63–65]). An important difference between the Hassanizadeh–Gray model and the Barenblatt model is that the latter includes nonequilibrium effects in *both* the capillary pressure and relative permeability. Bocharov

* Tel.: +1 617 253 7191.
E-mail address: juanes@mit.edu

0309-1708/$ - see front matter © 2008 Elsevier Ltd. All rights reserved.
doi:10.1016/j.advwatres.2007.12.005

et al. [66] presented one-dimensional numerical simulations using the Barenblatt model. A theoretical analysis of the nonequilibrium model was given by Natalini and Tesei [67]. Laboratory experiments to validate the model and determine the relevant parameters have recently been conducted [68,69]. All of these investigations are restricted, however, to two-phase flow.

The objective of this paper is to investigate, for the first time, the impact of nonequilibrium effects on predictions of *three-phase* flow models. We do so by

(i) Using Barenblatt's model with negligible capillary pressure. The focus is therefore on dynamic effects in the relative permeability, rather than capillary pressure (which has been studied more profusely in earlier investigations).
(ii) Numerical simulation. We develop an elegant and simple finite difference scheme to discretize a system of conservation laws (partial differential equations) coupled with closure evolution equations (ordinary differential equations). The scheme allows us to treat consistently and in a locally-conservative fashion the primary variables (actual saturations) and the hidden variables (effective saturations).

2. Nonequilibrium effects in multiphase flow

The traditional macroscopic formulation of multiphase flow in porous media hinges on a straightforward extension of Darcy's law that relates the volumetric flux of a phase to the pressure gradient of that phase:

$$\boldsymbol{q}_\alpha = -\frac{k_{r\alpha}}{\mu_\alpha}\mathbf{k}(\nabla p_\alpha - \rho_\alpha \boldsymbol{g}). \tag{1}$$

In the equation above, the subscript α indicates the fluid phase (oil, water, or gas), $\boldsymbol{q}_\alpha$ is the volumetric flux or Darcy velocity, μ_α is the fluid viscosity, p_α is the phase pressure, ρ_α is the phase density, $\boldsymbol{g}$ is the gravity vector, $\mathbf{k}$ is the absolute permeability of the medium, and $k_{r\alpha}$ is the relative permeability of the α-phase. Darcy-type formulations make the additional assumption that, for given experimental or field conditions, the relative permeabilities depend on the current fluid saturations S_α. Under these conditions, the relation among volumetric fluxes, fluid pressures and fluid saturations is algebraic.

Nonequilibrium (also called dynamic) effects have been invoked and incorporated into continuum descriptions of multiphase flow based on a number of arguments. The essential feature is that they generalize the algebraic relation governing fluid flux into an evolution equation. The origin of this type of formulation can be traced back to the Cattaneo extension of Fourier's law [70,71]. It stems from the observation that diffusion equations propagate information at infinite speed, which is deemed unphysical.

From a physical standpoint, the arrangement of fluids in the pore space requires some relaxation time to achieve a stable or equilibrium configuration during the displacement of one fluid by another through a porous medium [59,60,64].

Continuum formulations of multiphase flow in porous media have been derived from volume averaging of the mass and momentum conservation equations at the microscale [37,72–75]. The main conclusion from these mathematical developments is that the macroscopic equations of multiphase flow should include additional (nonequilibrium) terms. A reflection of this enhanced formulation is the concept of dynamic capillary pressure [8,38].

Experimentally, it has been observed that the capillary pressure–saturation curve under dynamic conditions (such as in single-step or multistep outflow experiments) is different from that of static conditions [39,40,42].

2.1. Hassanizadeh–Gray model

Based on thermodynamic arguments and volumetric averaging of the microscopic multiphase flow equations, Hassanizadeh and Gray [8,38] proposed that, in a two-fluid system, the dynamic capillary pressure P_c^{dyn} (that is, the instantaneous local difference between phase pressures) is related to the static capillary pressure P_c^{stat} (that is, the capillary pressure in a quasi-static displacement) as follows:

$$p_o - p_w \equiv P_c^{dyn} = P_c^{stat} - \tau_H(S_w)\frac{\partial S_w}{\partial t}. \tag{2}$$

In the equation above, p_o and p_w are the phase pressures of the nonwetting and wetting phases, respectively, and τ_H is a phenomenological coefficient that takes positive values and depends on the water saturation S_w. For a drainage process (the nonwetting phase displacing the wetting phase), the local time derivative of water saturation is negative ($\partial_t S_w < 0$) and, therefore, the dynamic capillary pressure is higher than the static one ($P_c^{dyn} > P_c^{stat}$), in agreement with experimental observations [39].

2.2. Barenblatt model

The Hassanizadeh–Gray model introduces nonequilibrium effects in the capillary pressure–saturation relationship, but does not address their impact on the relative permeability. Barenblatt's model [59,60] is a model of *both* nonequilibrium capillary pressure and relative permeability. An excellent account of the state of the art of nonequilibrium two-phase displacements is given in [64]. Although this work focuses on the Barenblatt model, it provides links to other approaches, such as the Hassanizadeh–Gray model and the full-tensor relative permeability approach [25–28].

The basis for Barenblatt's model may be summarized as follows. A multiphase displacement in porous media implies myriads of pore-scale rearrangements. The characteristic time (redistribution or relaxation time) for rearrangement of the flow networks can be substantial. As a result, the flux of each phase does not depend on the *cur-*

rent saturation S_w alone. The working assumption is that the instantaneous (dynamic) relative permeability and capillary pressure can be evaluated as their static counterparts, but at some *effective* saturation σ_w:

$$\begin{aligned} k_{rw}^{dyn}(S_w) &= k_{rw}^{stat}(\sigma_w), \\ k_{ro}^{dyn}(S_w) &= k_{ro}^{stat}(\sigma_w), \\ P_c^{dyn}(S_w) &= P_c^{stat}(\sigma_w). \end{aligned} \tag{3}$$

Closure of the model requires that one provides a relationship between the actual saturation S_w and the effective saturation σ_w. Using dimensional analysis and physical reasoning, Barenblatt proposed the following evolution (as opposed to algebraic) relation:

$$\sigma_w - S_w = \tau_B(S_w)\frac{\partial S_w}{\partial t}. \tag{4}$$

The effective saturation may be interpreted as a *future* saturation. Indeed, to first approximation:

$$\sigma_w \approx S_w(t + \tau_B), \tag{5}$$

highlighting the interpretation of the coefficient τ_B as relaxation time. Moreover, the phenomenological coefficients of the Hassanizadeh–Gray model and the Barenblatt model are related, to first order, by

$$\tau_H(S_w) \approx \left|\frac{dP_c^{stat}}{dS_w}\right| \tau_B(S_w). \tag{6}$$

In our view, τ is not explicitly time-dependent. However, since it multiplies the time derivative of saturation, $\partial_t S$ (Eq. (4)), nonequilibrium effects are important only where saturation changes are significant—the dynamic term decays, for example, after the front of a waterflood has passed. There is a great deal of uncertainty regarding the appropriate magnitude and functional form of the phenomenological coefficients [39,40,65]. In this investigation we adopt Barenblatt's model, as it incorporates nonequilibrium effects on both capillary pressure and relative permeability, and we extend it formally to three-phase flow systems.

3. Nonequilibrium two-phase flow models

We first describe the development of a numerical model for nonequilibrium effects in two-phase flow. In the next section, we extend the model to three-phase flow systems.

3.1. Darcy-type model

Let us make the following assumptions regarding the multiphase flow system: (1) two immiscible, incompressible fluids; (2) rigid medium; (3) one-dimensional horizontal flow. Under these assumptions, the Darcy-type two-phase flow model reads:

$$\partial_t S_\alpha + \partial_x v_\alpha = 0, \qquad \alpha = w, o, \tag{7}$$

$$v_\alpha = -\lambda_\alpha \frac{k}{\phi}\partial_x p_\alpha, \qquad \lambda_\alpha = \frac{k_{r\alpha}}{\mu_\alpha}. \tag{8}$$

Using a fractional flow formulation, the set of two mass conservation equations above may be expressed as a pressure equation and a saturation equation [76,77]. The pressure equation, obtained by summing the two conservation equations, dictates that the total velocity $v_T \equiv v_w + v_o$ depends on time only

$$\partial_x v_T = 0 \quad \Rightarrow \quad v_T = v_T(t). \tag{9}$$

The total velocity is given by

$$v_T = \lambda_T \frac{k}{\phi}\partial_x p - \lambda_w \frac{k}{\phi}\left(-\frac{dP_c}{dS}\right)\partial_x S, \tag{10}$$

where for convenience, we have introduced the notation: $p \equiv p_o$, $S \equiv S_w$, $P_c \equiv P_c^{stat} \equiv p_o - p_w$, and $\lambda_T = \lambda_w + \lambda_o$.

The saturation equation is the water-phase mass conservation equation, which we now express in conservation form as

$$\partial_t S + \partial_x\left[v_T f - f\lambda_o \frac{k}{\phi}\left(-\frac{dP_c}{dS}\right)\partial_x S\right] = 0, \tag{11}$$

where f is the water fractional flow function:

$$f = \frac{\lambda_w}{\lambda_T}. \tag{12}$$

3.2. Nonequilibrium model

Eq. (11) serves as the starting point for our nonequilibrium model. The essential point is to evaluate the flux term at the effective saturation σ rather than the actual saturation S:

$$\partial_t S + \partial_x\left[v_T f(\sigma) - f(\sigma)\frac{k_{ro}(\sigma)}{\mu_o}\frac{k}{\phi}\left(-\frac{dP_c(\sigma)}{d\sigma}\right)\partial_x \sigma\right] = 0, \tag{13}$$

together with the evolution equation:

$$\sigma - S = \tau \partial_t S. \tag{14}$$

We gain insight into the relative importance of the different terms by making the equations dimensionless. We introduce dimensionless space and time:

$$\hat{x} = \frac{x}{L}, \tag{15}$$

$$\hat{t} = \int_0^t \frac{v_T(t')}{L}dt', \tag{16}$$

where L is the length of the domain. If the total velocity v_T is constant, Eq. (16) reduces to $\hat{t} = t/T_c$, where $T_c = L/v_T$ is a characteristic time.

We introduce the Leverett scaling [78] of capillary pressure:

$$P_c(\sigma) = \frac{\gamma\cos\alpha}{\sqrt{k/\phi}}J(\sigma), \tag{17}$$

where γ is the interfacial tension, α is the contact angle, and J is a dimensionless function describing the capillary behavior of the porous medium under quasi-static condi-

tions (the Leverett J-function). This function is a monotonically decreasing function of saturation.

We define the capillary-diffusion function

$$D(\sigma) = f(\sigma)k_{\mathrm{ro}}(\sigma)(-J'(\sigma)), \tag{18}$$

which is a positive function except at the saturation endpoints, at which it takes a zero value.

3.2.1. Dimensionless form of the equations

The governing equations of the nonequilibrium model can now be written in dimensionless form as follows:

$$\partial_{\hat{t}} S + \partial_{\hat{x}}\left[f(\sigma) - \mathrm{Ca}^{-1}\frac{\sqrt{k/\phi}}{L}D(\sigma)\partial_{\hat{x}}\sigma\right] = 0, \tag{19}$$

$$\sigma - S = \hat{\tau}\partial_{\hat{t}} S. \tag{20}$$

The behavior of the system is governed by two dimensionless groups: the *capillary number*,

$$\mathrm{Ca} = \frac{\mu_{\mathrm{o}} v_{\mathrm{T}}}{\gamma\cos\alpha}, \tag{21}$$

and the *dimensionless relaxation time*,

$$\hat{\tau} = \tau\frac{v_{\mathrm{T}}}{L}. \tag{22}$$

The relative importance of capillary forces is, of course, inversely proportional to the capillary number and the length of the domain [79]. From Eq. (22), we conclude that nonequilibrium effects are proportional to the total velocity, and inversely proportional to the length of the domain. To have a sense for real-world values of τ, take the dimensionless value $\hat{\tau} = 0.01$ (this will be used later in this paper). For a lab experiment with $L \approx 1$ m and $v_{\mathrm{T}} \approx 1\ \mathrm{m\,h^{-1}}$, the corresponding value of the relaxation time is $\tau \approx 1$ min. For values representative of field conditions (say, $L \approx 100$ m and $v_{\mathrm{T}} \approx 0.1\ \mathrm{m\,day^{-1}}$), the relaxation time is $\tau \approx 10$ day.

3.2.2. Linearization

It is illustrative to derive the leading order terms in an expansion of the solution in the relaxation time $\hat{\tau}$, to show the dissipative nature of the relaxation. The static model ($\hat{\tau} = 0$) with capillarity is given by the equation:

$$\partial_{\hat{t}} S + \partial_{\hat{x}}\left[f(S) - \mathrm{Ca}^{-1}\frac{\sqrt{k/\phi}}{L}D(S)\partial_{\hat{x}} S\right] = 0. \tag{23}$$

Eq. (20) implies that

$$\varphi(\sigma) = \varphi(S) + \hat{\tau}\varphi'(S)\partial_{\hat{t}} S + \mathrm{O}(|\hat{\tau}|^2) \tag{24}$$

for any smooth function φ. The nonequilibrium model without capillarity can be approximated, to first order in $\hat{\tau}$, by the following equation:

$$\partial_{\hat{t}} S + \partial_{\hat{x}}\left[f(S) - \hat{\tau}(f'(S))^2\partial_{\hat{x}} S\right] = \mathrm{O}(|\hat{\tau}|^2). \tag{25}$$

Eqs. (23) and (25) are nonlinear advection–diffusion equations. It is clear that, to first order, nonequilibrium effects in the relative permeability act as a diffusion term that scales with the dimensionless relaxation time $\hat{\tau}$. The nonequilibrium–diffusion coefficient $\hat{\tau}(f'(S))^2$ is a positive function, except possibly at the endpoints—where it may take a zero value.

3.3. Summary of the model equations

We are interested in the nonequilibrium equivalent of the Buckley–Leverett model [3,67], so we consider the capillarity-free case ($P_{\mathrm{c}} = 0$). We abuse notation and drop the tilde, but still refer to the dimensionless form of the equations:

$$\partial_t S + \partial_x[f(\sigma)] = 0, \tag{26}$$

$$\sigma - S = \tau\partial_t S. \tag{27}$$

This is a system of a partial differential equation and an ordinary differential equation. We supplement this system with a flux boundary condition at the left boundary:

$$f(\sigma) = \bar{f}(t) \quad \text{at } x = 0. \tag{28}$$

The initial conditions of system (26)–(27) deserve special attention. Initial conditions must be specified for both the actual saturation and the effective saturation. Because both are linked by an evolution equation, they cannot be chosen independently. Substituting Eq. (26) into (27) and evaluating at $t = 0$, the initial conditions are given by

$$S = S_0(x) \quad \text{at } t = 0, \tag{29}$$

$$\sigma_0 + \tau\partial_x[f(\sigma_0)] = S_0(x). \tag{30}$$

Note that the initial effective saturation σ_0 is the solution of a one-sided boundary-value problem, and that it will be nonconstant even if the initial actual saturation S_0 is constant.

3.4. Numerical discretization

We develop a simple finite volume discretization for the numerical solution of the initial and boundary-value problem (26)–(30). The essential ingredient of the proposed numerical formulation is to consider the effective saturation as a local (internal, or hidden) variable within each gridblock. The immediate benefit is that the formulation is locally conservative. The numerical discretization employed here is different from that of previous numerical solutions dealing with nonequilibrium effects in porous media (e.g. [45,66]), where the evolution equation $\sigma = S + \partial_t S$ is inserted in the partial differential equation. This leads to higher-order terms with cross derivatives (∂_{xt} and ∂_{xxt}), which are more cumbersome to discretize consistently [45,66]. For seminal references in the area of discretization of hyperbolic conservation laws with stiff relaxation terms, see e.g. [80–83].

We discretize the spatial domain $\Omega = [0, L]$ into N nonoverlapping gridblocks Ω_i:

$$[0, L] \equiv \Omega = \bigcup_{i=1}^{N}\Omega_i, \qquad \Omega_i = [x_{i-1/2}, x_{i+1/2}]. \tag{31}$$

We assume, for simplicity, a regular grid with gridblock size δx. Similarly, let δt be the constant time step size. Discretization of the governing equations amounts to establishing discrete mass conservation at each gridblock i and time step $[t^n, t^{n+1}]$. Given the actual and effective saturations at time t^n, we must solve for the actual and effective saturations at time t^{n+1}. Discrete mass conservation dictates (see Fig. 1):

$$S_i^{n+1}\delta x = S_i^n \delta x + (f_{i-1/2} - f_{i+1/2})\delta t. \tag{32}$$

We use a single-point upstream and a generalized trapezoidal rule for evaluation of the discrete flux:

$$f_{i+1/2} = f(\sigma_i^{n+\theta}), \quad \text{where} \quad \sigma_i^{n+\theta} = \theta\sigma_i^{n+1} + (1-\theta)\sigma_i^n. \tag{33}$$

The parameter θ defines the degree of implicitness, ranging from $\theta = 0$ for Forward Euler (explicit) to $\theta = 1$ for Backward Euler (fully implicit). In all our simulations, we used the value $\theta = 0.5$, corresponding to a Crank–Nicolson scheme. It is important to note that the flux is a function of the effective saturation, not the actual saturation. The discrete coupled equations for cell i and time t^{n+1} read:

$$R_s|_i^{n+1} = \frac{\delta x}{\delta t}\left(S_i^{n+1} - S_i^n\right) + \left(f(\sigma_i^{n+\theta}) - f(\sigma_{i-1}^{n+\theta})\right) = 0, \tag{34}$$

$$R_\sigma|_i^{n+1} = \left(S_i^{n+\theta} - \sigma_i^{n+\theta}\right) + \frac{\tau(S_i^{n+\theta})}{\delta t}\left(S_i^{n+1} - S_i^n\right) = 0. \tag{35}$$

This results in an algebraic system of $2N$ equations, to be solved for the actual and effective saturations at time t^{n+1}. In our implementation, we used full Newton iteration for the solution of the nonlinear system.

3.5. Numerical examples

We illustrate the effect of the dynamic relative permeability with a waterflood simulation. Consider a medium initially filled with a nonwetting phase ($S_0 = 0$). Water is injected after time $t = 0$, so that $\bar{f} = 1$. We used quadratic relative permeabilities,

$$k_{\mathrm{rw}} = S^2, \quad k_{\mathrm{ro}} = (1-S)^2, \tag{36}$$

and a viscosity ratio $\mu_o/\mu_w = 2$. We assumed that the relaxation time τ is constant, and independent of water saturation. This is clearly a simplification, but it is sufficient to demonstrate the behavior of solutions when nonequilibrium effects are included.

The numerical solutions are shown in Fig. 2. The top figure shows the water saturation profile at time $t = 0.4$ for the equilibrium model ($\tau = 0$). This is the solution to the classical Buckley–Leverett problem. Any smearing is due to numerical diffusion.

The middle plot of Fig. 2 shows the actual (solid lines) and effective (dashed lines) saturations at times $t = 0$ and $t = 0.4$ for the nonequilibrium model with $\tau = 0.01$. We make the following remarks:

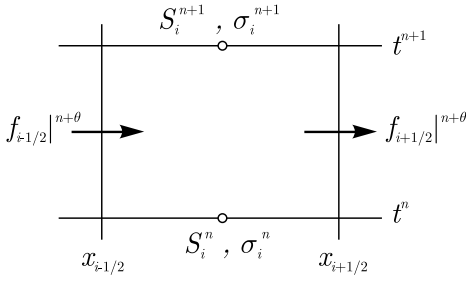

Fig. 1. Schematic of the finite volume discretization for the nonequilibrium two-phase flow model. The effective saturation σ is understood as an internal (hidden) variable within each gridblock.

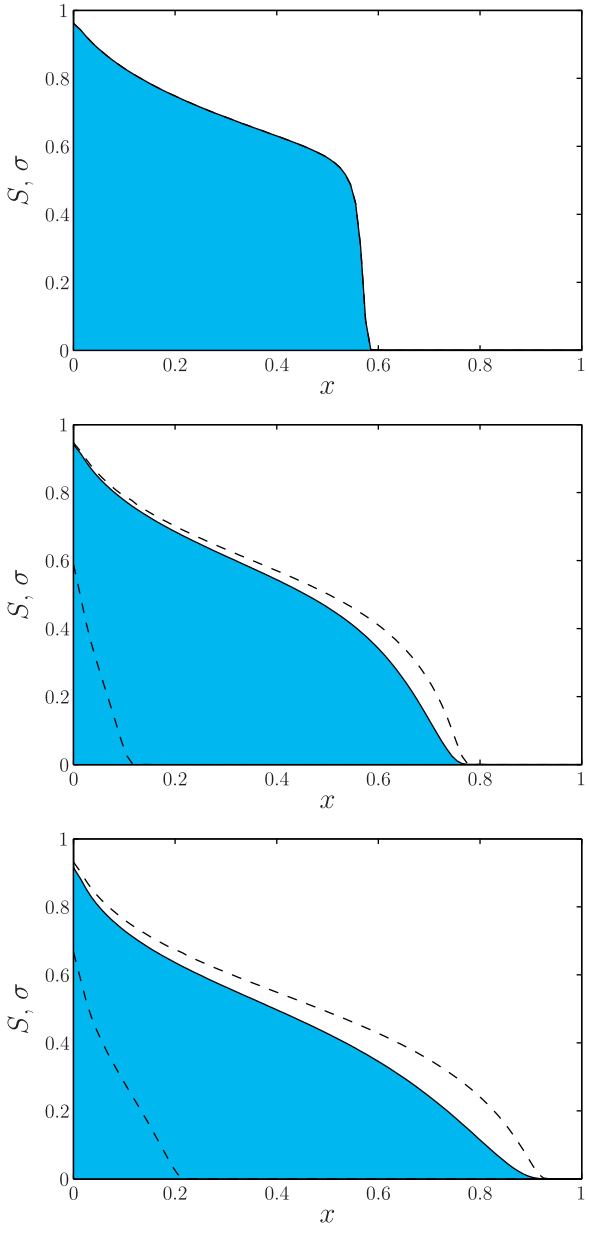

Fig. 2. Two-phase waterflood simulation. Profiles of actual saturation S (solid line) and effective saturation σ (dashed lines) at $t = 0$ and $t = 0.4$. Top: equilibrium model; middle: nonequilibrium model with $\tau = 0.01$; bottom: nonequilibrium model with $\tau = 0.02$.

(i) The initial effective saturation σ_0 is nonzero, even though $S_0 = 0$ everywhere. This behavior is not only mathematically correct, but also has a very physical interpretation: since σ is a "future" saturation, it must depend on the boundary conditions at $t = 0$.
(ii) The effective saturation front is always ahead of the actual front, which is consistent with the interpretation of the effective saturation as a "future" saturation.
(iii) The effect of the nonequilibrium term is to spread the front, even when capillary effects are ignored.

The bottom plot shows the computed profiles for the nonequilibrium formulation with a larger value of the relaxation time, $\tau = 0.02$. It is clear that this larger value of τ results in more significant spreading of the saturation front. Similar observations were made in the previous investigation by Bocharov et al. [66], although they used a very different numerical scheme.

4. Nonequilibrium three-phase flow models

In this section, we extend the nonequilibrium formulation proposed by Barenblatt to three-phase flow. We proceed as in the two-phase flow case, by introducing the Darcy-type formulation first, and then presenting the mathematical and numerical model that includes nonequilibrium effects.

4.1. Darcy-type model

We study three-phase flow under the usual fractional flow assumptions [84–87]: (1) three immiscible, incompressible fluids; (2) rigid medium; (3) one-dimensional horizontal flow; and (4) negligible capillarity effects. Under these conditions, the governing equations can be expressed in dimensionless form as a pressure equation:

$$\partial_x v_T = 0, \quad \text{where} \quad v_T = -\lambda_T \frac{k}{\phi} \partial_x p, \quad \lambda_T = \lambda_w + \lambda_o + \lambda_g, \tag{37}$$

and a 2×2 system of saturation equations which, after rescaling, takes the form

$$\partial_t \begin{pmatrix} S_w \\ S_g \end{pmatrix} + \partial_x \begin{pmatrix} f_w \\ f_g \end{pmatrix} = \begin{pmatrix} 0 \\ 0 \end{pmatrix}, \tag{38}$$

where $f_w = \lambda_w/\lambda_T$ and $f_g = \lambda_g/\lambda_T$ are the fractional flow functions for water and gas, respectively.

4.1.1. Elliptic regions

The system (38) is a 2×2 system of nonlinear first order equations in conservation form. The relative permeabilities are normally understood as functions of the fluid saturations alone. In this case, the mathematical character of the system is determined by the eigenvalues and eigenvectors of the Jacobian matrix of the system [88].

It is well known that most relative permeability models used today give rise to elliptic regions, that is, open sets in the saturation space where the system (38) is locally elliptic rather than hyperbolic [84,85,89–94]. There is a widespread controversy about whether elliptic regions are physical, or simply an unintended consequence of the severe modeling assumptions made in the development of three-phase flow models [84,85,91,95,96]. Here, we recall some of the repercussions of elliptic regions, and we study the effect of nonequilibrium terms on the solution to three-phase flow problems of mixed hyperbolic/elliptic type.

4.1.2. Dependence on initial data

The presence of elliptic regions in an otherwise hyperbolic three-phase flow model leads to a problem that is mathematically ill-posed. Entropy conditions have not been found to guarantee existence and uniqueness of a solution. Elliptic regions in saturation space are regions of linear instability. In particular, solutions do not depend continuously on the initial data.

To illustrate the lack of continuous dependence on initial data, we reproduce results from Bell et al. [90]. They used artificial relative permeability functions that produce a large elliptic region in saturation space, represented as a ternary diagram (each vertex corresponds to a single-phase system, see Fig. 3).

We solve the Riemann problem—that is, system (38) with constant initial and injected saturations—for injected and initial saturations (left and right states, respectively) inside the elliptic region:

$$\begin{pmatrix} S_w \\ S_g \end{pmatrix}_{\text{left}} = \begin{pmatrix} 0.16 \\ 0.29 \end{pmatrix}, \qquad \begin{pmatrix} S_w \\ S_g \end{pmatrix}_{\text{right}} = \begin{pmatrix} 0.15 \\ 0.30 \end{pmatrix}. \tag{39}$$

Note that the distance between left and right states on the ternary diagram is about 0.01. The solution (obtained using the numerical scheme described in Section 4.3) is shown in

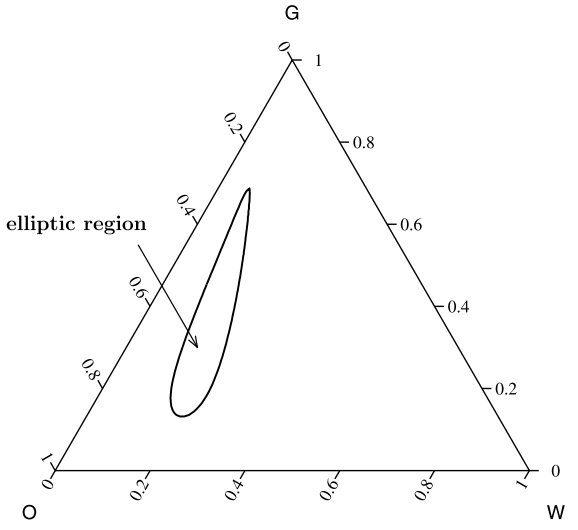

Fig. 3. Elliptic region on the ternary diagram (saturation space) corresponding to the relative permeability functions in [90].

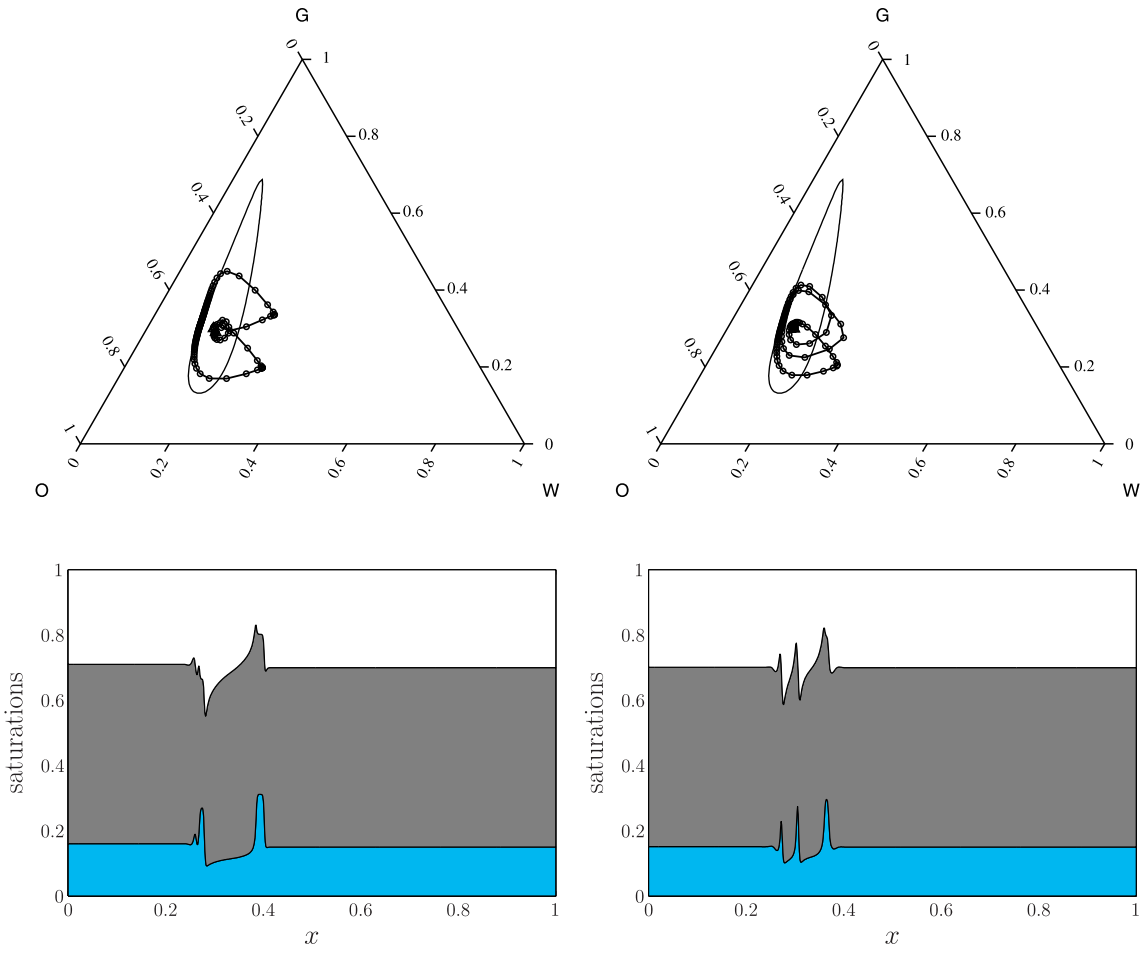

Fig. 4. Lack of continuous dependence of three-phase flow solutions on initial data inside the elliptic region (after [90]). Left: left and right states at a distance 0.01. Right: left and right states at a distance 0.001. The bottom figures show the water (light blue), oil (dark gray) and gas (white) saturation profiles. The top figures plot the same solutions as saturation paths on the ternary diagram.

Fig. 4(left). The grid was refined to ensure converged solutions. The bottom-left figure shows the saturation profiles (water in light blue[1], oil in dark gray, gas in white) after a certain simulation time. Despite the fact that initial and injected states are very close to one another, the solution develops a markedly oscillatory behavior due to the linear instability inside the elliptic region. The same solution is plotted as a path on the ternary diagram in the top-left figure. From these two plots, it is apparent that the solution develops two "spikes" or "constant states".

We now compute the solution for the same right state, and a left state that is even closer, at a distance of about 0.001:

$$\begin{pmatrix} S_w \\ S_g \end{pmatrix}_{\text{left}} = \begin{pmatrix} 0.151 \\ 0.299 \end{pmatrix}. \tag{40}$$

The solution is shown in Fig. 4(right). Clearly, the structure of the solution is different from the previous one. It now displays three "spikes" instead of two. From this example, taken from [90], we conclude that converged numerical solutions to the three-phase flow equations with initial data inside the elliptic region: (1) display wild nonoscillatory behavior, which we deem nonphysical, and (2) do not depend continuously on initial data.

4.2. Nonequilibrium model

In this section, we introduce a formal extension of Barenblatt's nonequilibrium model to three-phase porous media flow. The essence of the model is to evaluate the flux term (relative permeabilities and capillary pressures) at a set of effective saturations, different from the actual saturations. The two sets of saturations are linked by the following evolution equation:

$$\begin{pmatrix} \sigma_w \\ \sigma_g \end{pmatrix} - \begin{pmatrix} S_w \\ S_g \end{pmatrix} = \boldsymbol{\tau} \partial_t \begin{pmatrix} S_w \\ S_g \end{pmatrix}, \tag{41}$$

where $\boldsymbol{\tau}$ is now a 2×2 matrix of relaxation times with coefficients that depend, in principle, on water and gas saturations:

$$\boldsymbol{\tau} = \begin{pmatrix} \tau_{ww} & \tau_{wg} \\ \tau_{gw} & \tau_{gg} \end{pmatrix}, \qquad \tau_{\alpha\beta} = \tau_{\alpha\beta}(S_w, S_g). \tag{42}$$

[1] For interpretation of color in Figs. 2, 4–7, the reader is referred to the web version of this article.

Here, we propose that the relaxation time is a tensorial quantity, simply as a formal extension of the Barenblatt model to three-phase flow. The nature of this tensor is unknown. We speculate that it should have positive, real eigenvalues, in order to preserve the forward-in-time nature of the evolution Eq. (41). The simplest way to guarantee this property is to assume that this tensor be a diagonal tensor with uniformly positive coefficients. The coefficient τ_{ww} would correspond to an oil–water system, while the coefficient τ_{gg} would be associated with an oil–gas system.

For convenience, we define the following vector variables:

$$\boldsymbol{u} = \begin{pmatrix} S_w \\ S_g \end{pmatrix} \quad \text{(vector of actual saturations)}, \tag{43}$$

$$\boldsymbol{v} = \begin{pmatrix} \sigma_w \\ \sigma_g \end{pmatrix} \quad \text{(vector of effective saturations)}, \tag{44}$$

$$\boldsymbol{f} = \begin{pmatrix} f_w \\ f_g \end{pmatrix} \quad \text{(vector of fractional flows)}. \tag{45}$$

In the capillarity-free case, the nonequilibrium three-phase flow model is a strict extension of Eqs. (26)–(30). It is given by the PDE–ODE system:

$$\partial_t \boldsymbol{u} + \partial_x[\boldsymbol{f}(\boldsymbol{v})] = \boldsymbol{0}, \tag{46}$$

$$\boldsymbol{v} - \boldsymbol{u} = \boldsymbol{\tau}\partial_t \boldsymbol{u} \tag{47}$$

with the unilateral boundary conditions:

$$\boldsymbol{f}(\boldsymbol{v}) = \bar{\boldsymbol{f}}(t) \quad \text{at } x = 0, \tag{48}$$

and the initial conditions:

$$\boldsymbol{u} = \boldsymbol{u}_0(x) \quad \text{at } t = 0, \tag{49}$$

$$\boldsymbol{v}_0 + \boldsymbol{\tau}\partial_x[\boldsymbol{f}(\boldsymbol{v}_0)] = \boldsymbol{u}_0(x). \tag{50}$$

As for the two-phase case, the initial effective saturations $\boldsymbol{v}_0$ must be obtained through the solution of a one-sided boundary-value problem.

4.3. Numerical discretization

The numerical discretization of the model problem (46)–(50) is the strict equivalent of the two-phase numerical scheme, where now the actual and effective saturations are vector unknowns. We used a single-point upstream scheme for the space discretization, and a generalized trapezoidal rule for discretization in time. The vector of effective saturations is treated as an internal (hidden) variable, leading to a locally-conservative finite volume scheme.

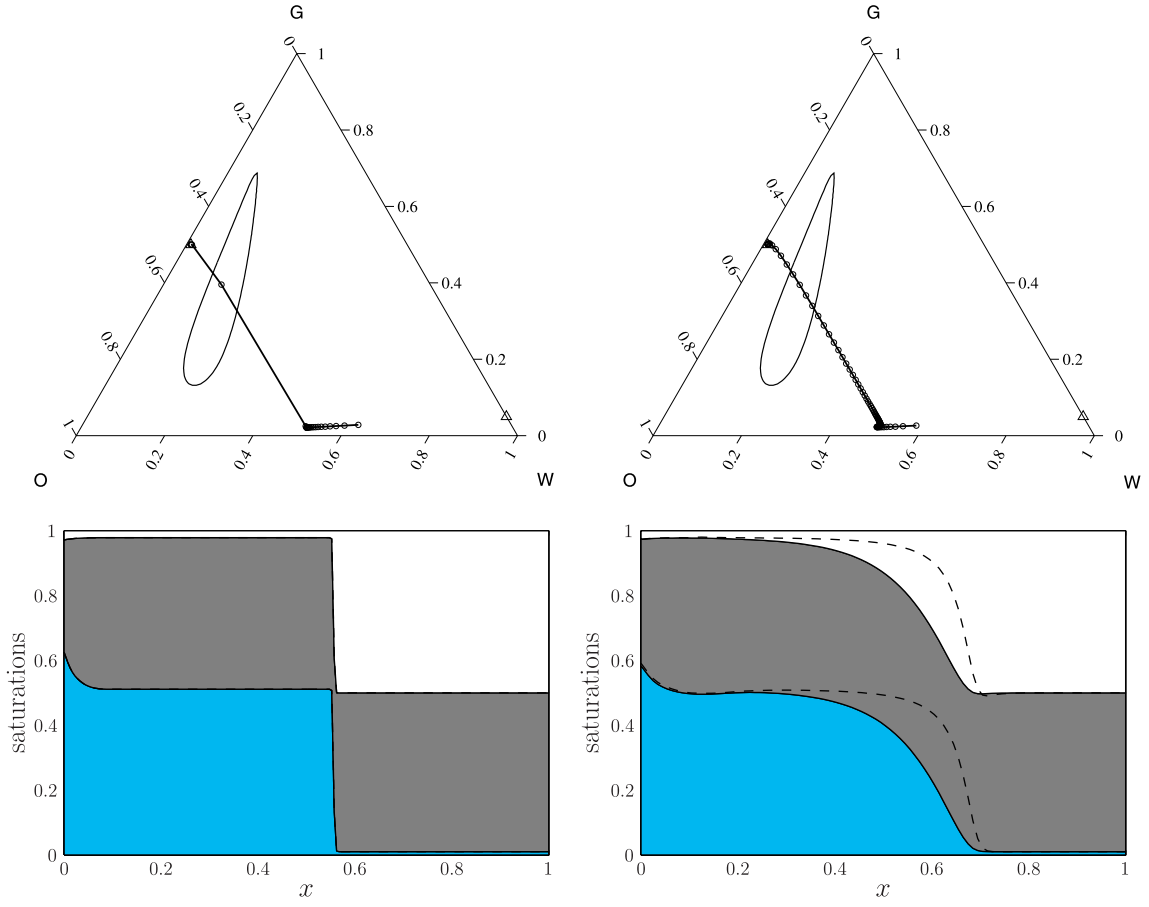

Fig. 5. Example 1: two states outside the elliptic region. Left: equilibrium formulation. Right: nonequilibrium formulation with $\tau = 0.02$. The dashed line indicates the profile of effective saturations.

The resulting $4N$-system of algebraic equations is solved at each time step using full Newton iteration.

4.4. Numerical examples

The objective of the numerical tests is to evaluate the impact of nonequilibrium effects on the behavior of solutions to three-phase flow problems. We are interested in three-phase models for which the equilibrium problem is of mixed hyperbolic/elliptic type. Specifically, we address the question of whether nonequilibrium effects stabilize the solution when the initial saturation states are inside the elliptic region.

All the numerical simulations are for problems with constant initial saturations ($\boldsymbol{u}_0 = \text{const}$), and constant boundary flux ($\bar{\boldsymbol{f}}(t) = \text{const}$). The relative permeabilities and fluid viscosities are taken from Bell et al. [90], which produce a large elliptic region (see Fig. 3). Given the uncertainty in the functional form of the relaxation time (which moreover is now a full matrix), we decided to use a scalar, constant τ.

4.4.1. Example 1

In this first example, we simulate a three-phase displacement in which both the initial and injected saturation states are outside the elliptic region. The results are shown in Fig. 5 for the equilibrium formulation (left) and the nonequilibrium formulation with $\tau = 0.02$ (right). The two solutions display a similar behavior in terms of saturation path, but the nonequilibrium model results in a smeared displacement front. As expected, the front of effective saturation (dashed line) is always ahead of the actual saturation front. These observations are in agreement with those of the two-phase flow case.

4.4.2. Example 2

In this example, the initial state is inside the elliptic region. The solution of the equilibrium model is perfectly well behaved, with the initial state being reached through a shock [90], see Fig. 6(left). The effect of the nonequilibrium term is qualitatively similar to that of Example 1: significant smearing of the solution profile, see Fig. 6(right).

4.4.3. Example 3

The final example is designed to illustrate the effect of dynamic relative permeability when both the initial and injected states are inside the elliptic region. The traditional Darcy-type formulation leads in this case to unstable oscillatory behavior and noncontinuous dependence on the ini-

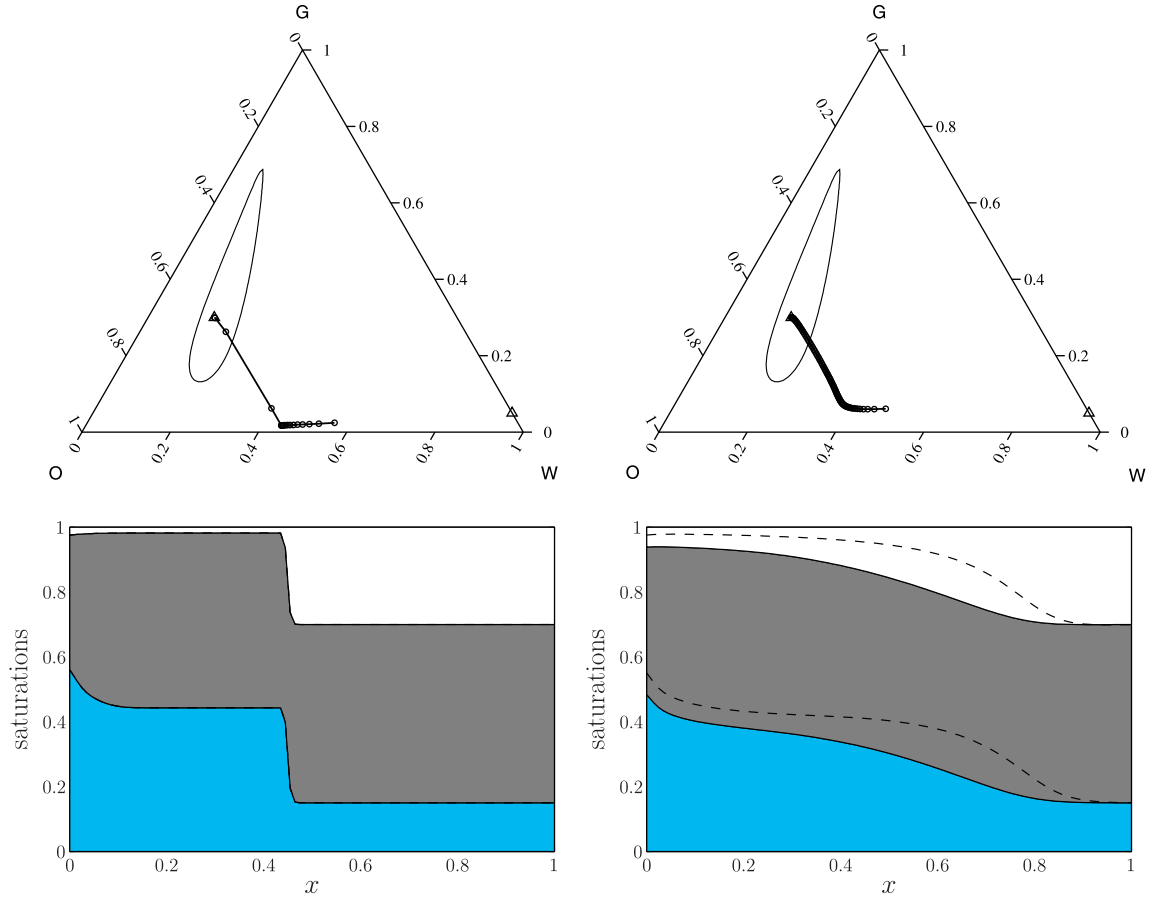

Fig. 6. Example 2: initial state inside the elliptic region. Left: equilibrium formulation. Right: nonequilibrium formulation with $\tau = 0.02$.

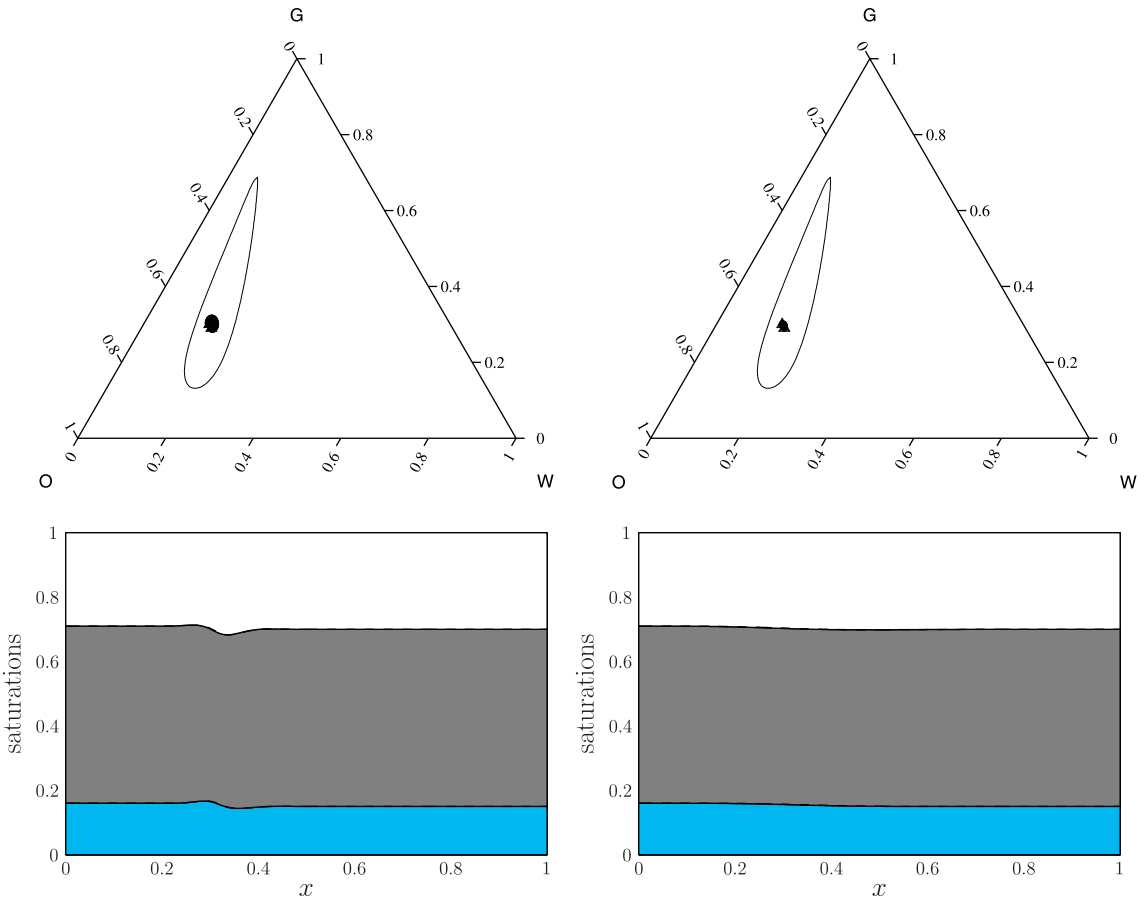

Fig. 7. Example 3: both states inside the elliptic region. Left: nonequilibrium formulation, $\tau = 0.01$. Right: nonequilibrium formulation, $\tau = 0.1$. These solutions should be compared with that of the equilibrium model in Fig. 4(left).

tial data, as discussed in Section 4.1.2. The question is: do nonequilibrium effects remedy this situation?

In Fig. 7 we show the solutions to the nonequilibrium model for values of $\tau = 0.01$ and 0.1. These solutions should be compared with those of the equilibrium model, in Fig. 4(left). It is apparent that the converged numerical solution of the nonequilibrium model is smooth and now remains inside the elliptic region. From this point of view, the solution displays a more physical behavior, although this appears to require a large-enough value of the relaxation time.

5. Concluding remarks

We have presented a nonequilibrium model of three-phase flow in porous media. The formulation is an extension of the model proposed by Barenblatt and co-workers for two-phase flow [59,60,64], and it includes dynamic effects in both the relative permeability and the capillary pressure functions of traditional Darcy-type formulations. The three-phase flow equations consist in a set of conservation laws (partial differential equations) coupled to a set of evolution equations (ordinary differential equations) that link the actual and effective fluid saturations. We have presented a consistent numerical method for the solution of this coupled system that treats effective saturations as internal variables, local to each element. The method is locally mass conservative, and its extension to several space dimensions is straightforward.

Our numerical simulations show that nonequilibrium terms smear saturation fronts. This had been previously observed for two-phase flow [66], and we have confirmed that the same is true for three-phase flow. What is more, they stabilize the solution inside the elliptic region—where the solution would otherwise be locally unstable and display wild oscillatory behavior. However, a sufficiently large magnitude of the characteristic relaxation time is required to damp out the oscillations. Similar findings were reported when capillarity effects are included [96]. This is in fact not surprising, as dynamic relative permeability introduce a mixed space–time derivative of saturation ($\partial_{xt}S$). To first order, this scales as a second-order derivative in space ($\partial_{xx}S$), which is the term associated with static capillary effects (see Section 3.2). In this context, it is worth mentioning that the higher-order terms associated with nonequilibrium effects allow one to recover uniqueness of nonmonotonic traveling wave solutions of infiltration into porous media [51].

The work presented here is subject to a number of interesting extensions:

(i) The numerical model can be extended to account for capillarity, also including nonequilibrium effects. This can be done using effective saturations, and without modification of the overall discretization scheme.
(ii) The main parameter of the formulation, the relaxation time, should be understood as a full-tensor whose coefficients are functions of the fluid saturations.
(iii) A logic to incorporate hysteresis in the relative permeability (such as [9]) should also be implemented.
(iv) The computational model can be extended to multidimensional problems in heterogeneous media using the same conservative scheme. We are currently undertaking this investigation.

References

[1] Richards LA. Capillary conduction of liquids through porous mediums. Physics 1931;1:318–33.
[2] Muskat M, Meres MW. The flow of heterogeneous fluids through porous media. Physics 1936;7:346–63.
[3] Buckley SE, Leverett MC. Mechanism of fluid displacement in sands. Petrol Trans AIME 1942;146:107–16.
[4] Bear J. Dynamics of fluids in porous media, environmental science series. New York: Elsevier; 1972. reprinted with corrections, New York: Dover; 1988.
[5] Abriola LM, Pinder GF. A multiphase approach to the modeling of porous media contamination by organic compounds, 1. Equation development. Water Resour Res 1985;21(1):11–8.
[6] Muskat M. Physical principles of oil production. New York: McGraw-Hill; 1949.
[7] Hassanizadeh SM. Derivation of basic equations of mass transport in porous media, Part 2. Generalized Darcy's and Fick's laws. Adv Water Resour 1986;9:207–22.
[8] Hassanizadeh SM, Gray WG. Toward an improved description of the physics of two-phase flow. Adv Water Resour 1993;16(1):53–67.
[9] Larsen JA, Skauge A. Methodology for numerical simulation with cycle-dependent relative permeabilities. Soc Pet Eng J 1998;3(2):163–73.
[10] Spiteri EJ, Juanes R. Impact of relative permeability hysteresis on the numerical simulation of WAG injection. J Pet Sci Eng 2006;50(2):115–39.
[11] Spiteri EJ, Juanes R, Blunt MJ, Orr Jr FM. Relative permeability hysteresis: trapping models and application to geological CO_2 sequestration. In: SPE annual technical conference and exhibition, Dallas, TX, 2005 [SPE 96448].
[12] Juanes R, Spiteri EJ, Orr Jr FM, Blunt MJ. Impact of relative permeability hysteresis on geological CO_2 storage. Water Resour Res 2006;42:W12418. doi:10.1029/2005WR004806.
[13] Spiteri EJ, Juanes R, Blunt MJ, Orr Jr FM. A new model of trapping and relative permeability hysteresis for all wettability characteristics. Soc Pet Eng J. [in press].
[14] Øren PE, Bakke S, Arntzen OJ. Extending predictive capabilities to network models. Soc Pet Eng J 1998;3(4):324–36.
[15] Øren PE, Bakke S. Process based reconstruction of sandstones and prediction of transport properties. Transp Porous Media 2002;46(2–3):311–43.
[16] Blunt MJ. Flow in porous media—pore network models and multiphase flow. Curr Opin Colloid Interface Sci 2001;6:197–207.
[17] Blunt MJ, Jackson MD, Piri M, Valvatne PH. Detailed physics, predictive capabilities and macroscopic consequences for pore-network models of multiphase flow. Adv Water Resour 2003;25:1069–89.
[18] Valvatne PH, Blunt MJ. Predictive pore-scale modeling of two-phase flow in mixed wet media. Water Resour Res 2004;40:W07406. doi:10.1029/2003WR002627.
[19] Piri M, Blunt MJ. Three-dimensional mixed-wet random pore-scale network modeling of two- and three-phase flow in porous media. I. Model description. Phys Rev E 2005;71. doi:10.1103/PhysRevE.71.026301.
[20] Piri M, Blunt MJ. Three-dimensional mixed-wet random pore-scale network modeling of two- and three-phase flow in porous media. II. Results. Phys Rev E 2005;71. doi:10.1103/PhysRevE.71.026302.
[21] Suicmez VS, Piri M, Blunt MJ. Pore-scale modeling of water alternate gas injection. Transp Porous Media 2007;66(3):259–86.
[22] Oak MJ. Three-phase relative permeability of water-wet Berea. In: SPE/DOE seventh symposium on enhanced oil recovery, Tulsa, OK, 1990. [SPE/DOE 20183].
[23] Egermann P, Vizika O, Dallet L, Requin C, Sonier F. Hysteresis in three-phase flow: experiments, modeling and reservoir simulations. In: SPE European petroleum conference, Paris, France, 2000 [SPE 65127].
[24] Element DJ, Masters JHK, Sargent NC, Jayasekera AJ, Goodyear SG. Assesment of three-phase relative permeability models using laboratory hysteresis data. In: SPE international improved oil recovery conference, Kuala Lumpur, Malaysia, 2003 [SPE 84903].
[25] Rose W. Measuring transport coefficients necessary for the description of coupled two-phase flow of immiscible fluids in porous media. Transp Porous Media 1988;3(2):163–71.
[26] Rose W. Coupling coefficients for two-phase flow in pore spaces of simple geometry. Transp Porous Media 1990;5(1):97–102.
[27] Kalaydjian F. A macroscopic description of multiphase flow in porous media involving spacetime evolution of fluid–fluid interface. Transp Porous Media 1987;2(6):537–52.
[28] Kalaydjian F. Origin and quantification of coupling between relative permeabilities for two-phase flows in porous media. Transp Porous Media 1990;5(3):215–29.
[29] Avraam DG, Payatakes AC. Flow regimes and relative permeabilities during steady-state 2-phase flow in porous-media. J Fluid Mech 1995;293:207–36.
[30] Avraam DG, Payatakes AC. Generalized relative permeability coefficients during steady-state 2-phase flow in porous-media, and correlation with the flow mechanisms. Transp Porous Media 1995;20(1–2):135–68.
[31] Avraam DG, Payatakes AC. Flow mechanisms, relative permeabilities, and coupling effects in steady-state two-phase flow through porous media. The case of strong wettability. Ind Eng Chem Res 1999;38(3):778–86.
[32] Valavanides MS, Payatakes AC. True-to-mechanism model of steady-state two-phase flow in porous media, using decomposition into prototype flows. Adv Water Resour 2001;24:385–407.
[33] Blunt M, King MJ, Scher H. Simulation and theory of two-phase flow in porous media. Phys Rev A 1992;46(12):7680–99.
[34] Dahle HK, Celia MA. A dynamic network model for two-phase immiscible flow. Comput Geosci 1999;3:1–22.
[35] Singh M, Mohanty KK. Dynamic modelling of drainage through three-dimensional porous materials. Chem Eng Sci 2003;58(1):1–18.
[36] Al-Gharbi MS, Blunt MJ. Dynamic network modeling of two-phase drainage in porous media. Phys Rev E 2005;71(1). doi:10.1103/PhysRevE.71.016308.
[37] Hassanizadeh SM, Gray WG. Mechanics and thermodynamics of multiphase flow in porous media including interphase boundaries. Adv Water Resour 1990;13(4):169–86.
[38] Hassanizadeh SM, Gray WG. Thermodynamic basis of capillary pressure in porous media. Water Resour Res 1993;29(10):3389–405.
[39] Hassanizadeh SM, Celia MA, Dahle HK. Dynamic effects in the capillary pressure–saturation relationship and its impact on unsaturated flow. Vadose Zone J 2002;1(1):38–57.
[40] O'Carroll DM, Phelan TJ, Abriola LM. Exploring dynamic effects in capillary pressure in multistep outflow experiments. Water Resour Res 2005;41(11):W11419. doi:10.1029/2005WR004010.
[41] DiCarlo DA. Experimental measurements of saturation overshoot on infiltration. Water Resour Res 2004;40(4):W04215. doi:10.1029/2003WR002670.

[42] Stauffer F. Time dependence of the relations between capillary pressure, water content and conductivity during drainage of porous media. In: IAHR symposium on scale effects in porous media, Thessaloniki, Greece, 1978.
[43] Dahle HK, Celia MA, Hassanizadeh SM. Bundle-of-tubes model for calculating dynamic effects in the capillary-pressure–saturation relationship. Transp Porous Media 2005;58(1):5–22.
[44] DiCarlo DA. Modeling observed saturation overshoot with continuum additions to standard unsaturated theory. Adv Water Resour 2005;28:1021–7.
[45] Helmig R, Weiss A, Wohlmuth BI. Dynamic capillary effects in heterogeneous porous media. Comput Geosci 2007;11(3):261–74.
[46] Beliaev AY, Hassanizadeh SM. A theoretical model of hysteresis and dynamic effects in the capillary relation for two-phase flow in porous media. Transp Porous Media 2001;43(3):487–510.
[47] Manthey S, Hassanizadeh SM, Helmig R. Macro-scale dynamic effects in homogeneous and heterogeneous porous media. Transp Porous Media 2005;58(1–2):5–22.
[48] Mirzaei M, Das DB. Dynamic effects in capillary pressure–saturations relationships for two-phase flow in 3D porous media: Implications of micro-heterogeneities. Chem Eng Sci 2006;62(7):1927–47.
[49] Das DB, Gauldie R, Mirzaei M. Dynamic effects for two-phase flow in porous media: fluid property effects. AIChE J 2007;53(10):2505–20.
[50] Cuesta C, van Duijn CJ, Hulshof J. Infiltration in porous media with dynamic capillary pressure: travelling waves. Eur J Appl Math 2000;11:381–97.
[51] DiCarlo DA, Juanes R, LaForce T, Witelski TP. Nonmonotonic traveling wave solutions of infiltration in porous media. Water Resour Res 2008;44:W02406. doi:10.1029/2007WR005975.
[52] Cuesta C, Hulshof J. A model problem for groundwater flow with dynamic capillary pressure: stability of traveling waves. Nonlin Anal 2003;52:1199–218.
[53] van Duijn CJ, Peletier LA, Pop IS. A new class of entropy solutions of the Buckley–Leverett equation. SIAM J Math Anal 2007;39(2):507–36.
[54] Eliassi M, Glass RJ. On the continuum-scale modeling of gravity-driven fingers in unsaturated porous media: the inadequacy of the Richards equation with standard monotonic constitutive relations and hysteretic equations of state. Water Resour Res 2001;37:2019–35.
[55] Eliassi M, Glass RJ. On the porous-continuum modeling of gravity-driven fingers in unsaturated materials: extension of standard theory with a hold-back–pile-up effect. Water Resour Res 2002;38(11). doi:1210.1029/2001WR001131, Art. No. 1234.
[56] Eliassi M, Glass RJ. On the porous continuum-scale modeling of gravity-driven fingers in unsaturated materials: numerical solution of a hypodiffusive governing equation that incorporates a hold-back–pile-up effect. Water Resour Res 2003:39. doi:1110.1029/2002WR001535, Art. No. 1167.
[57] Egorov AG, Dautov RZ, Nieber JL, Sheshukov AY. Stability analysis of gravity-driven infiltrating flow. Water Resour Res 2003:39. doi:1210.1029/2002WR001886, Art. No. 1266.
[58] Nieber JL, Dautov RZ, Egorov AG, Sheshukov AY. Dynamic capillary pressure mechanism for instability in gravity-driven flows; review and extension to very dry conditions. Transp Porous Media 2005;58:147–72.
[59] Barenblatt GI. Filtration of two nonmixing fluids in a homogeneous porous medium. Sov Acad Izv: Mech Gas Fluids 1971;5:857–64.
[60] Barenblatt GI, Vinnichenko AP. Non-equilibrium seepage of immiscible fluids. Adv Mech 1980;3(3):35–50.
[61] Barenblatt GI, Gilman AA. A mathematical model of non-equilibrium countercurrent capillary imbibition. Eng Phys J 1987;52(3):456–61.
[62] Barenblatt GI, Garcia-Azorero J, De Pablo A, Vazquez JL. Mathematical model of the non-equilibrium water–oil displacement in porous strata. Appl Anal 1997;65:19–45.
[63] Barenblatt GI, Entov VM, Ryzhik VM. Theory of fluid flows through natural rocks. Theory and applications of transport in porous media, vol. 3. Dordrecht: Kluwer; 1990 [expanded and revised edition of the original in Russian Dvizhenie zhidkostei i gazov v prirodnykh plastakh, Nedra Publishers; 1984].
[64] Barenblatt GI, Patzek TW, Silin DB. The mathematical model of non-equilibrium effects in water–oil displacement. Soc Pet Eng J 2003;8(4):409–16.
[65] Silin D, Patzek T. On Barenblatt's model of spontaneous countercurrent imbibition. Transp Porous Media 2004;54(3):297–322.
[66] Bocharov OB, Kuznetsov VV, Chekhovich YV. Numerical study of the nonequilibrium filtration of immiscible liquids. J Eng Phys 1989;57(1):803–6.
[67] Natalini R, Tesei A. On the Barenblatt model for non-equilibrium two phase flow in porous media. Arch Rational Mech Anal 1999;150(4):349–67.
[68] Le Guen SS, Kovscek AR. Nonequilibrium effects during spontaneous imbibition. Transp Porous Media 2006;63:127–46.
[69] Schembre JM, Kovscek AR. Estimation of dynamic relative permeability and capillary pressure from countercurrent imbibition experiments. Transp Porous Media 2006;65:31–51.
[70] Cattaneo C. A form of heat conduction equation which eliminates the paradox of instantaneous propagation. Comp Rend 1958;247:431–3.
[71] Compte A, Metzler R. The generalized Cattaneo equation for the description of anomalous transport processes. J Phys A – Math Gen 1997;30:7277–89.
[72] Hassanizadeh M, Gray WG. General conservation equations for multi-phase systems: 1. Averaging procedure. Adv Water Resour 1979;2(3):131–44.
[73] Hassanizadeh M, Gray WG. General conservation equations for multi-phase systems: 2. Mass, momenta, energy, and entropy equations. Adv Water Resour 1979;2(4):191–203.
[74] Hassanizadeh M, Gray WG. General conservation equations for multi-phase systems: 3. Constitutive theory for porous media flow. Adv Water Resour 1980;3(1):25–40.
[75] Gray WG, Hassanizadeh SM. Macroscale continuum mechanics for multiphase porous-media flow including phases, interfaces, common lines and common points. Adv Water Resour 1998;21:261–81.
[76] Aziz K, Settari A. Petroleum reservoir simulation. London: Elsevier; 1979.
[77] Chavent G, Jaffré J. Mathematical models and finite elements for reservoir simulation. Studies in mathematics and its applications, vol. 17. Elsevier, North-Holland; 1986.
[78] Leverett MC. Capillary behavior of porous solids. Petrol Trans AIME 1941;142:152–69.
[79] Zhou D, Fayers FJ, Orr Jr FM. Scaling of multiphase flow in simple heterogeneous porous media. In: SPE/DOE improved oil recovery symposium, Tulsa, OK, 1994. [SPE 27833].
[80] Pember R. Numerical methods for hyperbolic conservation laws with stiff relaxation I. Spurious solutions. SIAM J Appl Math 1993;53(5):1293–330.
[81] Pember R. Numerical methods for hyperbolic conservation laws with stiff relaxation II. Higher-order Godunov methods. SIAM J Sci Comput 1993;14(4):824–59.
[82] Jin S. Runge–Kutta methods for hyperbolic conservation laws with stiff relaxation terms. J Comput Phys 1995;122:51–67.
[83] Jin S, Levermore CD. Numerical schemes for hyperbolic conservation laws with stiff relaxation terms. J Comput Phys 1996;126:449–67.
[84] Juanes R. Displacement theory and multiscale numerical modeling of three-phase flow in porous media. PhD Dissertation, University of California at Berkeley [March 2003].
[85] Juanes R, Patzek TW. Relative permeabilities for strictly hyperbolic models of three-phase flow in porous media. Transp Porous Media 2004;57(2):125–52.
[86] Juanes R, Patzek TW. Analytical solution to the Riemann problem of three-phase flow in porous media. Transp Porous Media 2004;55(1):47–70.
[87] Juanes R, Patzek TW. Three-phase displacement theory: an improved description of relative permeabilities. Soc Pet Eng J 2004;9(3):302–13.

[88] Zauderer E. Partial differential equations of applied mathematics. Series in pure and applied mathematics. New York: John Wiley & Sons; 1983.
[89] Charny IA. Subterranean hydro-gas dynamics. Moscow: Gostoptekhizdat; 1963 [in Russian].
[90] Bell JB, Trangenstein JA, Shubin GR. Conservation laws of mixed type describing three-phase flow in porous media. SIAM J Appl Math 1986;46(6):1000–17.
[91] Shearer M, Trangenstein JA. Loss of real characteristics for models of three-phase flow in a porous medium. Transp Porous Media 1989;4:499–525.
[92] Holden L. On the strict hyperbolicity of the Buckley–Leverett equations for three-phase flow in a porous medium. SIAM J Appl Math 1990;50(3):667–82.
[93] Holden H. On the Riemann problem for a prototype of a mixed type conservation law. Comm Pure Appl Math 1987;40(2): 229–64.
[94] Holden H, Holden L, Risebro NH. Some qualitative properties of 2×2 systems of conservation laws of mixed type. In: Keyfitz BL, Shearer M, editors. Nonlinear evolution equations that change type. The IMA volumes in mathematics and its applications, vol. 27. New York: Springer-Verlag; 1990. p. 67–78.
[95] Azevedo AV, Marchesin D, Plohr B, Zumbrun K. Capillary instability in models for three-phase flow. Z Angew Math Phys 2002;53:713–46.
[96] Jackson MD, Blunt MJ. Elliptic regions and stable solutions for three-phase flow in porous media. Transp Porous Media 2002;48:249–69.